# Measuring the Fast and Slow Energy Release of Laser-Excited Aluminum / Graphene Oxide Composites

**Jennifer L. Gottfried, Chi-Chin Wu**
CCDC Army Research Laboratory
Weapons and Materials Research Directorate
Aberdeen Proving Ground, MD 21005
UNITED STATES
Email jennifer.l.gottfried.civ@mail.mil

**Xiaolin Zheng**
Stanford University
Department of Mechanical Engineering
Stanford, CA 94305
UNITED STATES

**Keywords: Aluminized; Defense; Energetic; Explosive; Graphene Oxide; Measurement.**

## ABSTRACT

*Graphene Oxide (GO) has been used to facilitate the oxidation of micron- and nano-sized aluminum (Al) particles on both the microsecond- and millisecond-timescales relevant to detonation chemistry and combustion performance, respectively. A laboratory-scale technique based on the pulsed laser excitation of milligram quantities of material was used to evaluate the energy release from the Al/GO composites. High-speed video images of the reacting materials and time-resolved emission spectra provided further insight into the differences in chemistry between the samples. Transmission Electron Microscopy (TEM) was used to characterize the structures and spatial distribution of elemental species for the Al/GO composite samples. Micron-Al/GO and nano-Al/GO demonstrated enhanced energy release on both the fast and slow timescales compared to pure micron-Al and nano-Al. Mixtures of the Al/GO composites (20 wt %) with the military explosive Trinitrotoluene (TNT) suggest that unlike conventional aluminized explosives, Al/GO composites have the potential to increase the detonation performance as well as providing enhanced blast effects.*

## 1.0 INTRODUCTION

Because of its high specific energy (31 kJ/g) and widespread availability, micron-sized aluminum (micron-Al) powders have been extensively used in energetics applications, primarily for blast enhancement on extended timescales (i.e., following the formation of detonation products). A key goal in energetic materials research is to accelerate the reaction of metals during an explosion so that the detonation performance of the explosive is enhanced. In addition to reacting too slowly to influence the detonation performance, micron-Al particles often suffer from incomplete combustion. Nano-sized Al (nano-Al) particles have the potential to react faster due to the increased specific surface area and kinetics-based (rather than diffusion-limited) reaction times, but suffer from issues such as the formation of a native oxide layer (alumina; $Al_2O_3$), which delays the reaction of the Al core and contributes significantly to the total mass of nano-Al particles, and strong agglomeration of the particles resulting in incomplete combustion.

Various approaches to improving the combustion efficiency and oxidation rate of Al have been investigated by our group and many others, including replacing the oxide layer with a more energetically favorable passivation layer [1], [2], [3], ball-milling the Al with faster-reacting metal species [4], formulation with energetic binders [5], and manipulation of the particle morphology [6], [7]. Because the oxidation of Al in an energetic formulation on a microsecond-timescale results in the Al scavenging oxygen (O) from the detonating explosive and reducing the detonation velocity [8], [9], enhancement of the detonation properties of an aluminized explosive requires additional oxidizing species in the formulation to maintain the optimal oxygen balance for the detonating explosive.

Graphene Oxide (GO) is typically synthesized by reacting graphite powders with strong oxidizing agents such as sulfuric acid ($H2SO_4$) and potassium permanganate ($KMnO_4$); the resulting GO sheets consisting of ordered nanoscale sp2 carbon domains, highly disordered oxidized sp3 domains, and carbon vacancy defects are functionalized with various carboxylic acid, phenol, hydroxyl, and epoxide groups [10]. While GO is an important precursor for the large-scale synthesis of graphene, GO has many interesting and unique properties as well [11], [12]. GO can be viewed as either molecules (along the ~1 nm nanometer-thick edge) or particles (along the active surface/basal plane, up to hundreds of micrometers).

Of particular interest for this work is the energetic nature of GO, which has been shown to undergo disproportionation reactions at 200 °C (~30% mass loss and ~1.3 kJ/g heat release under both air and argon [13]), resulting in the formation of reduced-GO, heat, and gases [14], [15]. GO contaminated with alkali salts from the chemical synthesis process is highly flammable in air, producing additional heat and gas due to carbon combustion reactions at 500°C (~40% mass loss and ~8.9 kJ/g heat release). GO has been demonstrated as an effective catalyst for various reactions [16], [17], [18], [19], [20], [21], [22]. Table 1 gives an overview of some of the energetic applications of GO that have been explored.

**Table 1: Example Energetic Applications of GO.**

| Reference | Sample/Formulation | Description of results |
|---|---|---|
| Brodie [23] | GO | First report of the thermal instability of GO. |
| Croft [24] | GO | Also noted the thermal instability of GO upon heating. |
| Boehm and Scholz [25] | GO | Reported combustion of GO upon heating. |
| Jimenez [26] | GO | Measured the thermal decomposition of GO. |
| Sabourin et al. [27] | Nitromethane/GO | GO catalyzed nitromethane combustion, leading to lower ignition temperatures and increased burning rates. |
| Kim et al. [28] | GO | Observed spontaneous ignition of GO contaminated with potassium (K) in air. |
| Krishnan et al. [10] | GO | Demonstrated that the thermal instability of GO is due to the presence of alkali impurities such as K or sodium (Na). |
| Li et al. [29] | Cyclotetramethylene tetranitramine (HMX)/GO | GO decreased the impact and friction sensitivity of HMX and increased the thermal stability. |
| Zhang et al. [30] | Nitrocellulose (NC)/GO | GO added to enhance the optical ignition with a Nd:YAG laser and increase the burning rate of NC; also increased the thermal stability. |
| Zhang et al. [31] | Nitromethane/GO | Molecular dynamics simulations showing the mechanisms for catalytic decomposition of hot nitromethane by GO. |
| Liu et al. [32] | Hexanitrohexaaza-isowurtzitane (HNIW or CL-20)/GO | GO found to have no significant effect on the thermal properties of CL20. |
| Yu et al. [33] | CL-20/binder/GO | GO was found to slightly decrease the impact and friction sensitivity of the CL-20/binder, lower the decomposition temperature, increase the heat of decomposition, and decrease the critical explosion temperature during slow cook-off tests. |
| Qiu et al. [34] | GO | Observed explosive decomposition of GO samples in inert gas during thermal reduction, leading to laboratory equipment damage; 0.04 wt% K lowers the onset temperature for GO reduction and increases the probability for explosive reduction; increasing the sample mass enables the internal build-up of heat and gas, leading to thermal runaway in quantities as small as a few milligrams. |
| Thiruvengadathan et al. [35] | $BiO_3$/Al/GO | GO used to direct the self-assembly of Al and $Bi_2O_3$ nanoparticles, resulting in nearly double the energy release. |
| Thiruvengadathan et al. [36] | $BiO_3$/Al/GO | GO used to direct the self-assembly of Al and $Bi_2O_3$ nanoparticles, resulting in enhanced pressure generation, pressurization rate, burning rate, and specific impulse. |

| | | |
|---|---|---|
| Chen et al. [37] | Metal nanoparticles / reducedGO films | Developed process to uniformly distribute reactive metal nanoparticles in a reduced-GO film; demonstrated energetic properties of nano-Al embedded in reduced-GO, which served as a barrier to oxidation and agglomeration for the Al. |
| Qiu et al. [38] | GO | Concluded that the explosive thermal decomposition of GO is a function of mass; for higher masses, the reaction rates exceed heat losses to the surrounding environment, leading to thermal runaway. |
| Memon et al. [39] | GO / Ammonium Perchlorate (AP) / Hydroxyl-Terminated Polybutadiene (HTPB) | Used recrystallization / fast crash method to create AP/GO composite, which resulted in increased propellant burning rates at high pressures. |
| Wang et al. [40] | HMX/Viton/GO | GO desensitized HMX: improved thermal stability, lower impact and shock wave sensitivities. |
| Yan et al. [41] | GO/energetic materials | Review of GO (and other functionalized carbon nanomaterials) in energetic compositions, with emphasis on Chinese literature. |
| Yan et al. [42] | Al@$Fe_2O_3$/GO | $Fe_2O_3$ deposited on GO/Al substrates via atomic layer deposition results in reduction of GO and formation of energetic composites with increased energy release and reduced electrostatic discharge sensitivity. |
| Yan et al. [43] | rGO@$Fe_2O_3$/AP | Reduced GO decorated with $Fe_2O_3$ nanoparticles was used to catalyze the decomposition of AP. |
| Tao et al. [44] | Al/CuO/GO | GO quantum dots (<100 nm in lateral dimensions) used as building blocks to assemble metastable intermolecular composites of Al and CuO, resulting in increased energy release and specific heat. |
| Wang et al. [45] | TKX-50/GO | GO changed the morphology of TKX-50, decreased the impact and friction sensitivities, and did not affect the thermal stability. |
| An et al. [46] | GO/Triaminoguanidine (TAG)/AP | Transition metal complexes of TAG nitrate with GO as a dopant were used to catalyze the decomposition of AP. |
| Jiang et al. [13] | micron-Al/GO | Micron-Al wrapped in GO to increase the optical ignition of Al with a Xe flash tube, also increased combustion efficiency. |
| Lyu et al. [47] | GO-doped PVDF/CuO/Al | Electrospinning the GO-doped nanocomposites improved the heat of reaction, density, and anti-oxidation capability compared to mechanical mixing, while GO improved the reaction efficiency of PVDF/CuO/Al. |
| Chen et al. [48] | GO/TAG | Transition metal complexes of TAG nitrate with GO as a dopant were used to investigate the mechanisms for GO stabilization of energetic materials. |
| Lakhe et al. [49] | GO | Demonstrated that GO can explosively decompose at normal drying temperatures with pressure generation rates >1000s psig/min, with surface area determining the critical mass necessary for decomposition. |
| Zhang et al. [50] | GO/TAG | Studied decomposition of GO/TAG via Reactive Force-Field (ReaxFF) with experimental validation; GO decreases the decomposition temperature of TAG. |
| Chen et al. [51] | GO/TAG/AP | Transition metal complexes of TAG nitrate with GO were used to study the decomposition of AP; the photon transfer between O and $O_2$ determines the catalytic decomposition pathways, depending on the reactive center. |
| Cheng et al. [52] | Functionalized-GO/AP | The effect of surface functional groups on metal-free GO energetic performance, thermal stability, and catalytic properties with respect to AP was investigated. |
| Hanafi et al. [53] | Functionalized-GO/AP or RDX | Highly energetic coordination polymers were synthesized by cross-linking functionalized GO; these polymers had a strong catalytic effect on the decomposition of AP and stabilized RDX. |
| Huang et al. [54] | GO/CL-20 | GO used to improve the thermal stability and decrease the mechanical sensitivity of CL-20 composites. |
| Qi et al. [55] | GO/energetic materials | Investigated the compatibility of various GO-related systems with energetic materials such as AP, RDX, and HMX. |
| Jiang et al. [56] | micron-Al/GO/ Fluorinated Graphene (FG) | GO facilitates the dissociation of FG, and FG accelerates the disproportionation and oxidation of GO; together, they greatly accelerate Al combustion. |

The enhancement of the ignition and combustion properties of micron-Al particles with as little as 3 wt % GO was recently demonstrated [13]. In addition to enabling micron-sized Al to be ignited by an optical Xenon (Xe) flash, the GO also promoted the more efficient combustion of Al in air on the millisecond-timescale. Analysis of the combustion reactions, post-combustion products, and reactive molecular dynamics simulations confirmed that the addition of GO promotes the oxidation of micron-Al particles via additional heat release (from exothermic disproportionation and oxidation reactions), catalytic effects (by providing active sites for stabilization of free radicals), and gas generation ($CO_2$, $H_2O$, etc.). The goal of this work was to determine if the exothermic disproportionation of GO and reactions of the resulting gaseous products could be used to facilitate the oxidation of micron-Al and/or nano-Al on the microsecond-timescale in order to improve the detonation performance of military explosives.

A laser-based technique developed at the Combat Capabilities Development Command's (CCDC) Army Research Laboratory (ARL) for evaluating the energetic performance of milligram quantities of material was used to measure the energy release of Al/GO composites on both the fast (i.e., detonation-relevant) and slow (i.e., propellant/blast-related) timescales. The Laser-Induced Air Shock From Energetic Materials (LASEM) technique uses a high energy, nanosecond-pulsed laser to ablate, atomize and excite a residue material, forming a laser-induced plasma with temperatures exceeding 10,000 K [57]. The heating rate and microsecond-timescale conditions in the laser-induced plasma are very similar to those during detonation initiation and within the chemical reaction zone behind a detonation front during an explosion, respectively. Just as reactions behind the detonation front drive a shock wave through the bulk material, the high-temperature reactions in the laser induced plasma increase the velocity of the laser-induced shock wave that expands into the air above the sample; thus, the more energetic the material is on the microsecond-timescale, the faster the resulting laser induced shock velocity [58]. On the millisecond-timescale, the intensity and duration of combustion (or deflagration) reactions indicate the potential of the material for propellant-based applications [59]. The LASEM method for estimating detonation performance has been demonstrated for conventional military explosives [58], novel energetic materials [60], military explosives with added Al or boron [9], and novel metal additives [1], [2], [3], [61]. For both conventional [58] and aluminized [9] military explosives, the laser-induced shock velocities from LASEM can be directly correlated to the detonation velocity from large-scale detonation testing. Here, we compare the energy release rates for micron-Al/GO and nano-Al/GO powders and estimate the detonation performance of TNT mixtures with 20% added Al/GO.

## 2.0 EXPERIMENTAL

### 2.1 Synthesis of Al/GO Composites

Al/GO composites (80/20 wt %) were prepared by mechanical mixing, also known as ultrasonic mixing. The Al particles were either an average 3.9 µm or 70 nm in diameter. The Al was sonicated in a 1:1 dimethylformamide and isopropyl alcohol solution (10 mg/mL) for 15 min. The GO powder (0.55 – 1.2 nm thick, 0.5 – 3 µm diameter) was sonicated in dimethylformamide (1 mg/mL) for 2 hours. The two suspensions were then mixed and sonicated for 1 hour, filtered, heated at 100 °C for 1 hour to vaporize the solvent residue, and dried in a vacuum desiccator overnight [13].

### 2.2 Sample Imaging and Elemental Map Acquisition

Transmission Electron Microscope (TEM) specimens were prepared via a standard nanoparticle suspension technique by dispersing a small quantity of Al/GO in acetonitrile and sonicating until a colloidal solution was formed. A few drops of the Al/GO-containing solution were then added onto the holey carbon film-supported TEM grid (Ted Pella; 300 mesh) and air dried. The samples were studied using a JEOL 2100FX microscope operated at a 200 kV acceleration voltage (JEOL USA, Inc.). The samples were imaged under Bright Field (BF) image conditions with a Gatan Digital Micrograph and an Orius digital camera (Gatan, Inc.). The

chemical analyses were performed by acquiring elemental X-ray maps of the nano-Al/GO derived from spectrum images acquired using the TEAM Analysis software (EDAX, Inc.) in the Scanning Transmission Electron Microscopy (STEM) mode.

## 2.3 LASEM Measurements

The LASEM technique has been described in detail previously [57], [58], and the configuration for this work is shown in Figure 1. Briefly, a 6-ns pulsed laser (1064 nm, 850 mJ) was focused below the sample surface. The laser ablates, atomizes, ionizes, and excites the sample – resulting in the generation of a laser-induced plasma. The heating rate and plasma conditions (temperature, pressure, electron density, etc.) are very similar to those occurring during the initiation and within the propagating chemical reaction zone of detonating energetic materials, respectively. The high-temperature reactions in the laser-induced plasma are monitored using time resolved, gated emission spectroscopy with an echelle / Intensified Charge Coupled Device (ICCD) spectrometer (200 – 1000 nm, 0.02-nm resolution). The formation of the laser-induced plasma generates a laser-induced shock wave, which expands into the air above the sample. A high-speed color camera records the expansion of the shock wave via schlieren imaging [62] at 84,000 frames-per-second (1 µs shutter). Exothermic chemical reactions occurring in the plasma during the expansion of the shock wave through the plasma region (<10 µs) increase the plasma temperature and accelerate the shock wave (which rapidly decays to the speed of sound in air following cessation of the laser pulse). The characteristic laser-induced shock wave for the sample under the given experimental conditions is determined by the y-intercept of a 5th order polynomial fit of the shock wave velocity versus time.

Particles ejected off the sample surface by the laser-induced shock wave can start combusting as they pass through the region of air heated by the plasma and the passage of the shock wave. These self-sustained combustion reactions, which occur on the millisecond-timescale, are monitored with a second time-resolved emission spectrometer (230 – 900 nm, 0.25-nm resolution) and photodiodes that are

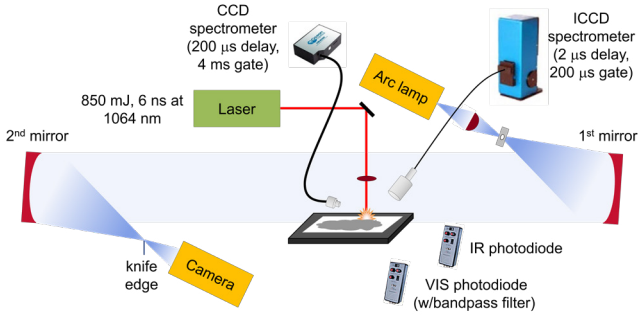


Figure 1: Experimental Schematic for the Laser Ablation and Excitation of Al/GO Composites Using LASEM. The emission from the laser-induced plasma and subsequent combustion reactions was detected with spectrometers gated to the appropriate time regime and time-resolved emission integrated over the Visible (VIS) and Infrared (IR) wavelengths was recorded with photodiodes. The laser-induced shock wave was recorded with a high-speed camera using schlieren imaging.

integrated over the infrared (900 – 1700 nm) or visible (300 – 1050 nm) emission regions. A bandpass filter at 486 nm was added to the visible photodiode to monitor the AlO emission during the combustion reactions.

In addition to the Al/GO composites prepared for this work, LASEM data on the 70 nm Al precursor for the nano-Al/GO composites was obtained; previous data on a micron-Al sample [9] and a commercial GO was used. The military explosive Trinitrotoluene (TNT) was obtained from colleagues at ARL and hand-mixed with the Al additives (20% by weight) for comparison to the tritonal formulation of TNT with 20% micron-Al previously studied [4]. All samples were prepared by spreading a thin layer of material on double-sided tape affixed to a glass microscope slide (~100 µg/mm$^2$). While the laser-induced shock velocities are independent of the material thickness (since excess material is ejected off the sample slide out of the laser-material interaction region), the extent and duration of the millisecond-timescale combustion reactions depends strongly on the residue thickness [2] – thus the sample thicknesses were kept as consistent as possible between samples and between different sample slides.

# 3.0 RESULTS

## 3.1 TEM Analyses

For the micron-Al/GO composite, the morphology and structural features of the

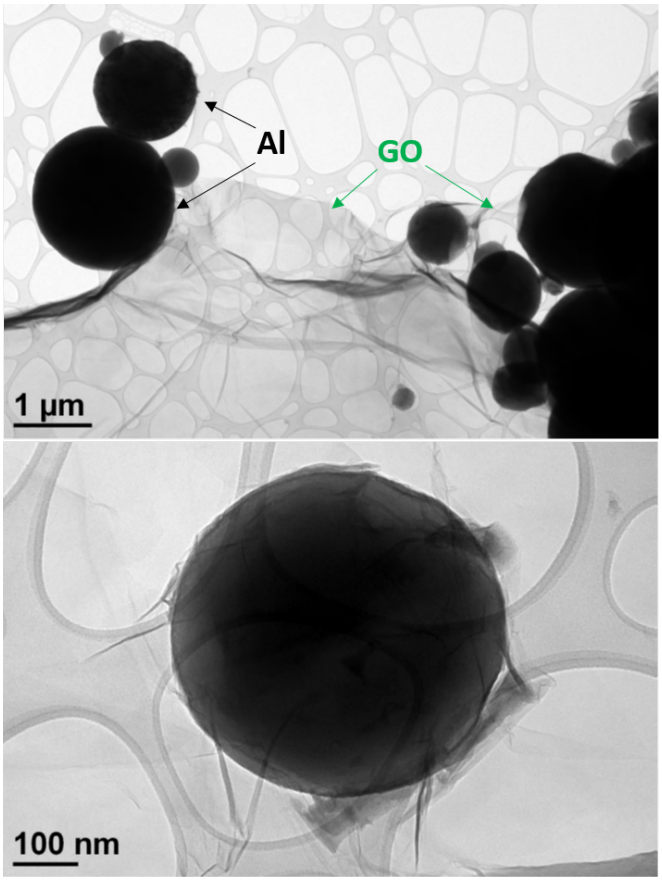


Figure 2: TEM Images of Micron-Al/GO Showing Inconsistent Particle Wrapping with the GO. Recorded with a high-speed camera using schlieren imaging.

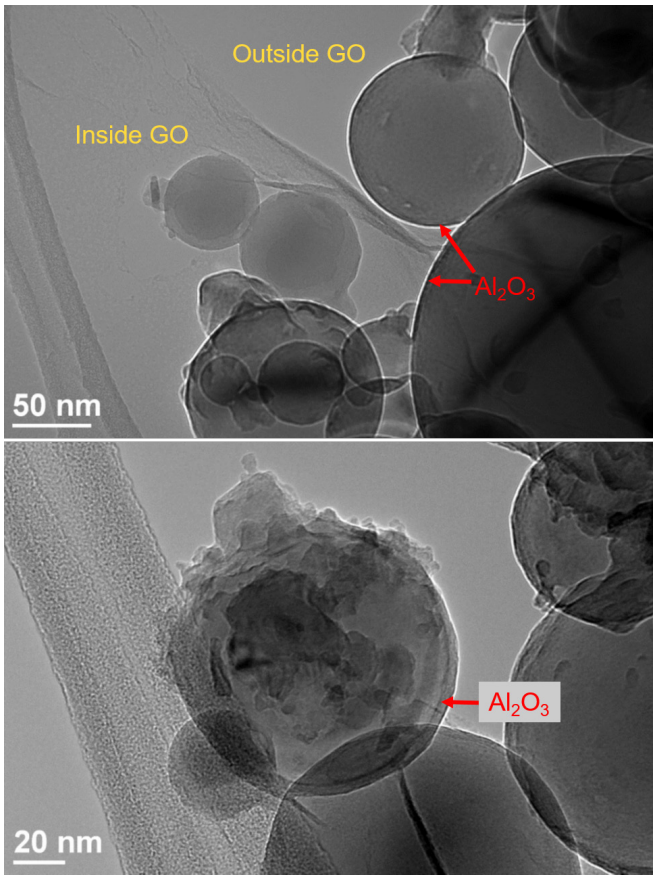


Figure 3: TEM Images of Nano-Al/GO Showing the Wrapping of the GO Sheets Around The Nano-Al, the Presence of the $Al_2O_3$ Shell, and the Contamination Present on Some of the Al Particle Surfaces.

micron-Al particles cannot be fully revealed in TEM because of the relatively large particle diameters, which make the sample opaque to electrons; a typical thickness for an electron-transparent specimen is usually less than 100 nm. Scanning Electron Microscope (SEM) images of the micron-Al/GO composites were previously published [13]. After surveying many different regions with TEM, we found that GO wrapping was not successful for most micron-Al particles. As shown in Figure 2, complete wrapping of the micron-Al/GO was only achieved for smaller Al particles, e.g., the approximately 500 nm Al particle shown in the bottom of Figure 2. This can be attributed to direct spatial blocking effects due to the relatively large particle sizes. The difficulty in GO wrapping was also exacerbated due to the presence of agglomerated micron-Al, as shown in the top right of Figure 2.

On the other hand, detailed structural features were revealed in TEM for the nano-Al/GO particles because they were much more electron beam transparent. The amorphous $Al_2O_3$ shell surrounding the crystalline Al core was clearly visible with different contrasts in the TEM images (Figure 3). The nano-Al/GO particles had better surface coverage of the nano-Al by the GO. The white rings in the images shown in Figure 3 indicate an under focus condition, which was chosen to show the strong contrast of the crystalline Al core. Surface contamination on the nano-Al/GO particles resulting in "Christmas ornament"-like particles was also observed sporadically. The source of the observed impurities in nano-Al/GO composites is not yet clear. However, the contaminants may have been introduced during the sonication process used for the sample preparation.

In order to further characterize the wrapping of the nano-Al particles with the GO and the origin of the observed structural features, elemental maps of the nano-Al/GO sample were obtained via STEM Mode in TEM (Figure 4). These elemental maps show the presence of nitrogen (N), which is seemingly concentrated near the particle-particle

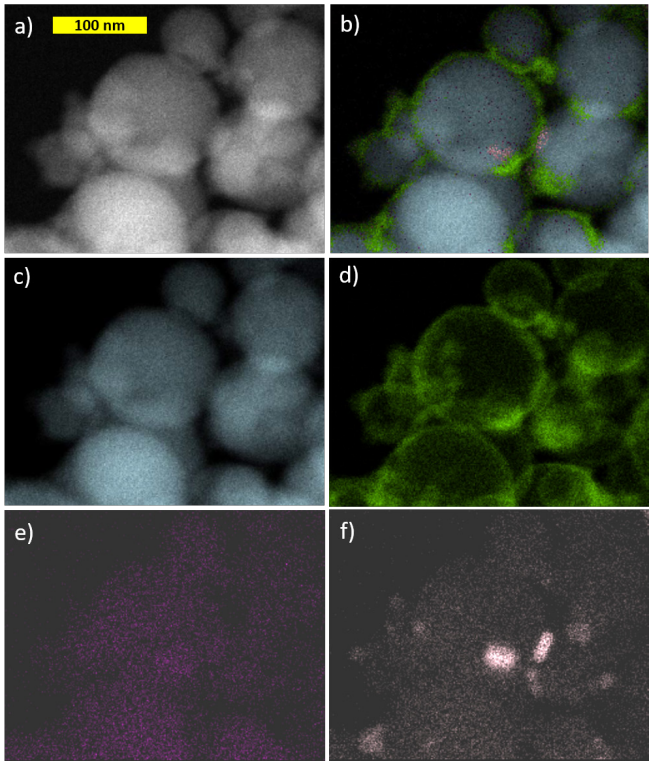


Figure 4: (a) TEM Image and (b) the Corresponding Elemental Map Obtained Using STEM Showing the Spatial Distributions of (c) Aluminum, (d) Oxygen, (e) Carbon, and (f) Nitrogen in Nano-Al/GO.

interfaces and O on the surface of the nano-Al particles (from the native $Al_2O_3$ layer and/or the GO). Nitrogen can be introduced into the nano-Al particles during the commercial synthesis process. While a longer collection time was needed to obtain a stronger carbon (C) signal, the C (from GO and/or surface functional groups) appears well-dispersed throughout the nano-Al particles.

## 3.2 Emission Spectra

Time-resolved emission spectra from the laser-induced plasma of excited Al/GO composites provide information about the elemental composition of the ablated material, a technique known as Laser-Induced Breakdown Spectroscopy (LIBS) [63]. The LASEM setup

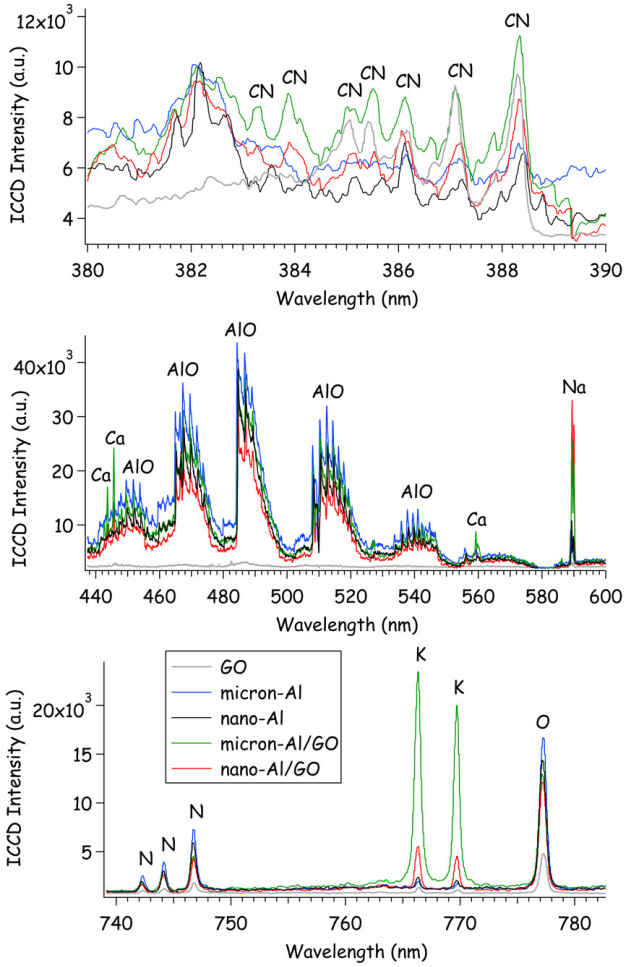


Figure 5: Emission Spectra integrated over the first 200 µs of the Laser-induced Plasma Lifetime (following a 2 µs delay to avoid the Broadband Continuum Emission).

incorporates LIBS as part of the diagnostic information collected. Previous work by Serrano et al. demonstrated the characterization and discrimination of graphite, graphene, and GO samples with LIBS [64]. Selected regions of the emission spectra of the GO, Al, and Al/GO samples are shown in Figure 5. Carbon emission is present in all the spectra, including Al; C in the Al spectra is a result of organic surface functional groups and/or organic impurities. The molecular Cyano (CN) radical emission, formed primarily from the recombination of C and N atoms in the plasma

**Table 2: Emission Intensity Ratios (with 95% Confidence Intervals) from the Spectra of GO, Al, and Al/GO Composites.**

| Sample | O/N | H/C | CN/C | Al/O | AlO/Al | Na/C | K/C |
|---|---|---|---|---|---|---|---|
| GO | 4.4 ± 1.0 | 2.5 ± 0.5 | 4.8 ± 2.0 | -- | -- | 0.82 ± 0.37 | 0.35 ± 0.29 |
| micron-Al | 2.5 ± 0.2 | 7.1 ± 1.6 | 1.9 ± 0.8 | 1.3 ± 0.2 | 1.0 ± 0.1 | 5.9 ± 2.7 | 0.63 ± 0.38 |
| nano-Al | 2.7 ± 0.3 | 5.3 ± 1.2 | 2.3 ± 0.5 | 1.4 ± 0.1 | 1.1 ± 0.3 | 6.7 ± 3.5 | 0.65 ± 0.99 |
| micron-Al/GO | 6.0 ± 0.2 | 3.4 ± 0.9 | 4.8 ± 1.0 | 0.58 ± 0.06 | 4.9 ± 1.0 | 14 ± 4 | 14 ± 3 |
| nano-Al/GO | 5.4 ± 1.0 | 10 ± 4 | 9.6 ± 3.6 | 0.87 ± 0.14 | 2.7 ± 0.5 | 55 ± 28 | 8.2 ± 4.2 |

(including N from air), is significantly stronger for the GO-containing samples. In the previous study [64], $C_2$ emission was not observed in the GO spectra (over a much shorter gate, 0.5 µs) – here, we have observed only very weak $C_2$ emission in the GO spectra over the 200 µs gate (near 516 nm). Depletion of $C_2$ radicals through competitive reactions with O in the plasma has been shown to reduce or eliminate $C_2$ emission from carbon-containing molecules [65]. While the presence of Al may promote the formation of $C_2$ (by preferentially reacting with the available O and reducing the formation of CO and $CO_2$), unfortunately any $C_2$ emission in the Al/GO composites is obscured by the strong aluminum monoxide (AlO) emission. All sample spectra also contain significant hydrogen (H) emission (not shown). The presence of hydrogen gas during the reduction of GO has been shown to result in violent reactions with –OH groups on GO surface [66], inducing thermal decomposition. Thus, increasing the hydrogen concentration in the composite material could potentially lead to GO decomposition reactions even faster. Hydrogen bonds also serve as bridges between adjacent nanosheets within the GO lattice [67].

While most of the O and N emission is due to entrainment of air into the laser-induced plasma, the O/N ratio (using background-corrected emission intensities) is higher for the GO-containing samples (Table 2) – which may serve as an indication of the extent of oxidation of the GO compared to other graphene-related samples. Higher O/C content has also been shown to increase the decomposition rate of GO [68], although in this case the C in the Al samples contributes significantly to this ratio. The AlO emission is only present in the Al-containing samples and indicates the extent of aluminum oxidation on the microsecond-timescale. The Al/O and AlO/Al ratios indicate that the Al/GO composites have less unoxidized Al in the first 200 µs of the reactions compared to pure Al particles.

In addition to the emission from the primary elemental species (C, Al, O), emission from impurities was also observed. The Al/GO composites contain higher concentrations of the alkali [lithium (Li), sodium (Na), and potassium (K)] and alkaline earth [magnesium (Mg), calcium (Ca), and strontium (Sr)] metals.

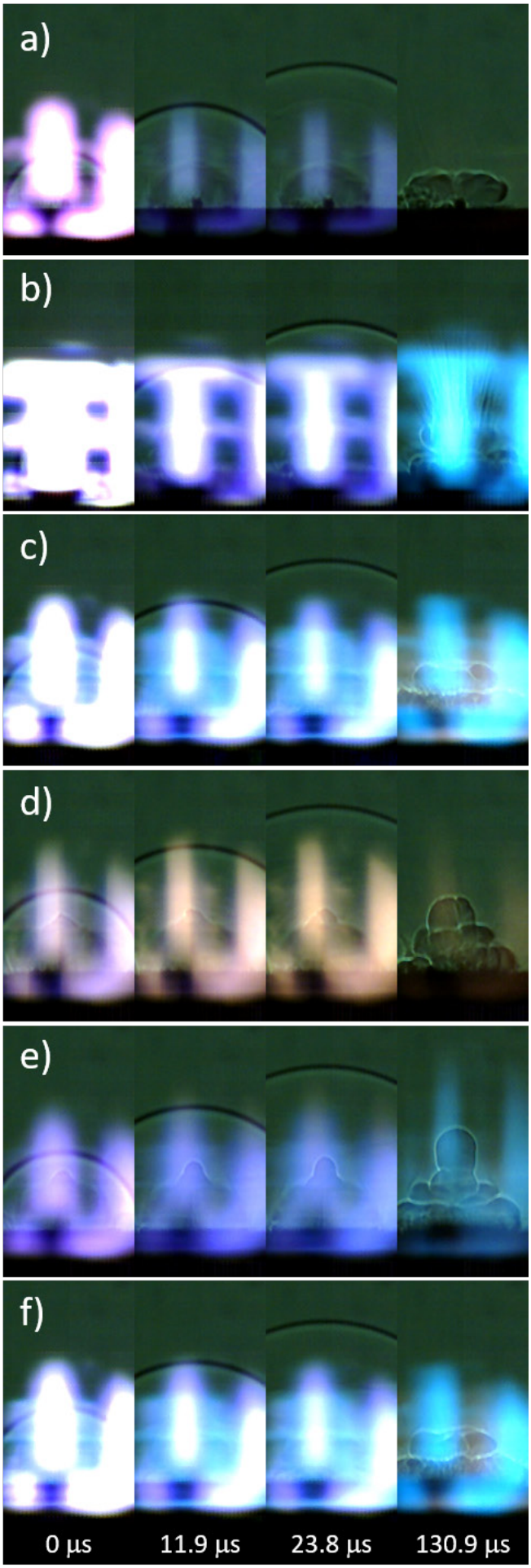


Figure 6: Snapshots from the High-Speed Video of Laser-Excited (a) Blank Tape, (b) Micron-Al, (c) Nano-Al, (d) GO, (e) Micron-Al/GO, and (f) Nano-Al/GO.

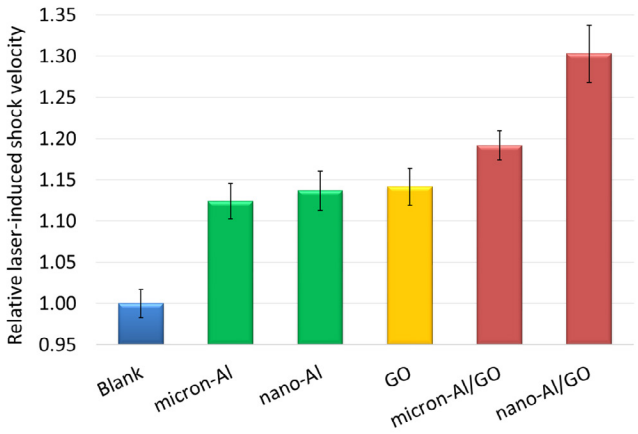


Figure 7: Relative Laser-Induced Shock Velocities for the Blank Tape Substrate, Micron-Al, Nano-Al, GO, and the Micron-Al/GO and Nano Al/GO Composites.

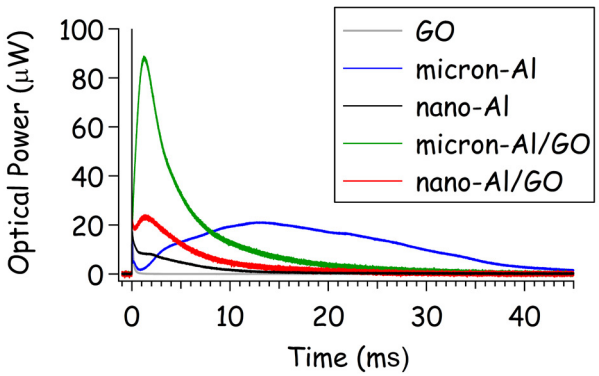


Figure 8: Emission from the Laser-Induced Plasma (1st Sharp Spike Near Time Zero) and the Subsequent Combustion Reactions of the GO, Al, and Al/GO Particles Ejected Into the Air Above the Sample Surface.

It is important to note that the pure GO and Al samples were similar, but not identical, to the materials used to make the Al/GO composites – so the impurities in the Al/GO composites could have originated from the starting components and were not necessarily introduced during the synthesis process. Because each laser shot samples only tens of micrograms of material, the concentration of these impurities (e.g., K) can vary significantly from shot-to-shot. Since alkali impurities are known to catalyze the decomposition of GO and increase flammability [10], the relative quantities of these impurities could potentially be used to evaluate the safety of GO-containing composites. For this application, where the heat released from the exothermic reactions of GO facilitates the oxidation of Al, the presence of the alkali salt contaminants may actually increase the efficiency of this process since they promote the further combustion of the reduced-GO products – thus enhancing the total energy release from GO.

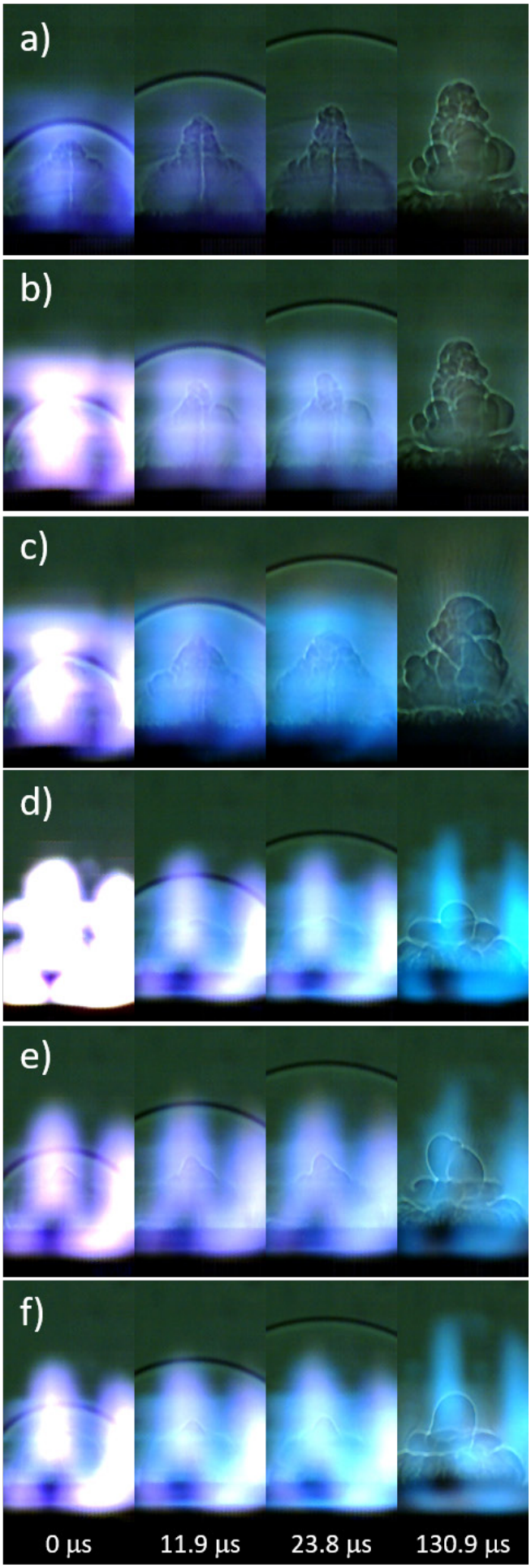


Figure 9: Snapshots from the High-Speed Video of Laser-Excited (a) TNT, (b) TNT+$Al_2O_3$, (c) TNT+micron-Al, (d) TNT+nano-Al, (e) TNT+micron-Al/GO, and (f) TNT+nano-Al/GO.

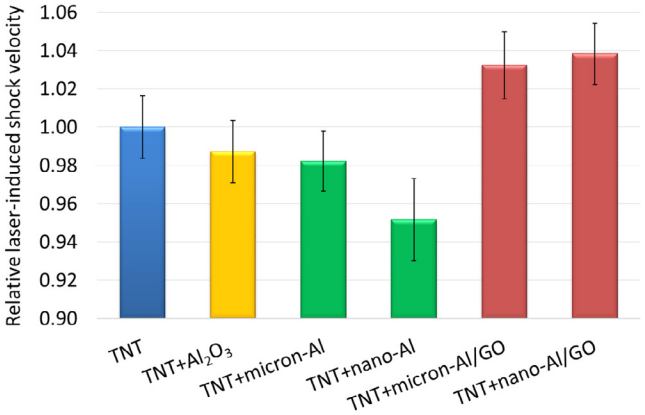


Figure 10: Relative Laser-Induced Shock Velocities for Pure TNT, TNT+$Al_2O_3$, TNT+micron-Al, TNT+nano-Al, TNT+micron-Al/GO, and TNT+nano-Al/GO.

## 3.3 Laser-Induced Shock Waves

Snapshots from the high-speed video of the laser excitation of the blank tape, micron-Al, nano-Al, GO, micron Al/GO, and nano-Al/GO are shown in Figure 6. All images have been cropped (from the top) and the brightness enhanced (+40%) to increase the contrast of the shock wave and background. In general, inert materials produce significantly more visible plasma emission [57]. Blue emission from AlO is visible in the images from Al-containing samples, purple CN emission appears in the GO-containing samples – as does the orange-ish Na emission from combustion of the GO at later times. The ejection of burning Al particles is visible in the micron-Al image at 130.9 µs (Figure 6(b), appearing as dark streaks). Significant differences in the plume expansion can be observed for the samples at later times, as shown in the last frame used to measure the shock position (130.9 µs, shock wave position cropped out-of-frame). Understanding the observed differences in plume expansion would require modelling the hydrodynamic

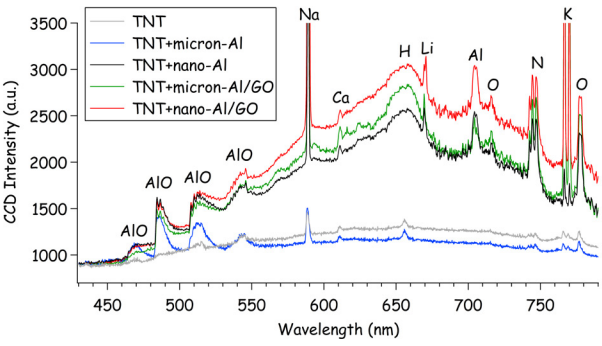


Figure 12: Emission Spectra for TNT, TNT+Al, and TNT+Al/GO Samples Integrated Over the First 4 ms of the Combustion Reactions Following the Laser-Induced Plasma.

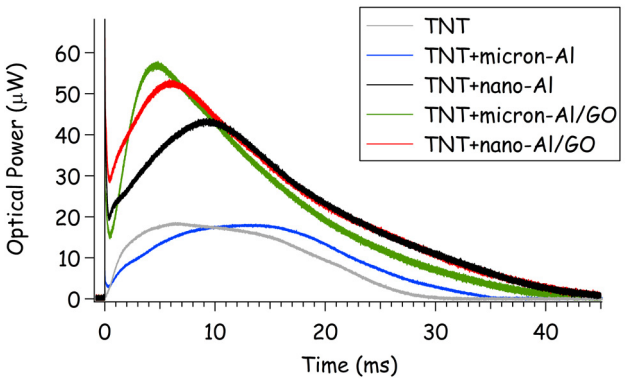


Figure 11: Emission from the Laser-Induced Plasma (1st Sharp Spike Near Time Zero) and the Subsequent Combustion Reactions of TNT, TNT+Al, and TNT+Al/GO Particles Ejected Into the Air Above the Sample Surface.

effects resulting from the high-temperature chemical reactions, which is beyond the scope of this study.

## 3.4 Energy Release Rates

The microsecond-timescale energy release rates (<10 µs), as measured by the laser-induced shock velocities, are shown in Figure 7. The energy release from micron-Al, nano-Al, and GO was exothermic compared to the inert blank tape substrate. Enhanced microsecond-timescale energy release was observed for the Al/GO composites compare to the pure Al samples. The energy release from nano-Al/GO was significantly higher than that of micron-Al/GO, as a result of the higher specific surface area of the nano-Al and/or more intimate contact between the Al and GO.

In contrast, the nano-Al/GO had less millisecond-timescale energy release than micron-Al/GO, as measured by the combustion emission (Figure 8). There are two contributions to this behavior:

1. Because the oxide layer comprises a more significant fraction of the mass of the nano-Al, it has a lower active Al content and thus less overall energy to release; and
2. Because the nano-Al reacts earlier, most of the Al had reacted by the time the combustion reactions occur.

Both Al/GO composites combust significantly faster and more strongly than their pure Al counterparts.

## 3.5 TNT+Al/GO Composites

In order to investigate the effect of the enhanced microsecond timescale reactions of the Al/GO composites on the detonation performance of TNT, mixtures of 20% by weight additive were prepared and tested. Images from the high-speed videos of laser-excited TNT, TNT+Al2O3, TNT+micron-Al, TNT+nano-Al, TNT+micron-Al/GO, and TNT+nano-Al/GO are shown in Figure 9. The characteristic laser-induced shock velocities for the samples are shown in Figure 10. While the addition of the inert Al2O3 reduces the laser-induced shock velocity of TNT (and thus the estimated detonation velocity), the micron-Al and nano-Al further reduce the estimated detonation velocity of TNT since the oxidation of the Al that reacts on the microsecond-timescale scavenges the O from the detonation products [8], [9]. Since the nano-Al is more reactive on the microsecond-timescale due to its larger specific surface area, this effect is more extreme than for the micron-Al. On the other hand, both the micron-Al/GO and nano Al/GO increase the estimated detonation velocity of TNT, suggesting that they contribute to the exothermic energy release without scavenging O from the detonation products – likely as a result of the O available due to the disproportionation reactions of GO. Interestingly, no significant difference in the laser-induced shock velocities between TNT+micron-Al/GO and TNT+nano Al/GO was observed, perhaps suggesting that the increased reactivity of the nano-Al is not sufficiently balanced by the presence of additional oxidizing agents from the GO.

In addition to the predicted increase in detonation performance by the Al/GO composites compared to Al, the increase in millisecond-timescale combustion observed for the composites (Figure 11) suggest that significantly enhanced blast effects may also be possible. The time to peak combustion is also faster for the Al/GO composites than Al. Unlike the emission spectra from the high-temperature laser-induced plasma (Figure 5), the combustion emission spectra are dominated by emission from molecular species and blackbody radiation from the burning particles (Figure 12). The Na and K emission from the TNT+Al/GO composites nearly saturate the spectrometer at ~12,000 counts each (off-scale).

## 4.0 CONCLUSIONS

By wrapping micron-Al and nano-Al in GO via sonication, enhanced energy release on both the microsecond and millisecond-timescales has been demonstrated. We speculate that the heat released from the exothermic disproportionation reactions of GO during rapid heating facilitate the oxidation of Al. Furthermore, the gases also released (e.g., CO, $CO_2$) reduce the agglomeration of product species that could have otherwise inhibited efficient combustion. According to the TEM analyses, efficient GO wrapping was achieved for nano-Al particles but not for the majority of the micron-Al particles – resulting in considerably different energy release rates between these two composites. The nano-Al/GO had significantly enhanced microsecond-timescale energy release. Further studies are needed to quantify the effect of alkali impurities on the catalytic effect of GO and improve the wrapping efficiency, especially for micron-Al particles. An improved methodology for preparing transmission transparent micron-Al/GO TEM specimens is also necessary to study their detailed structural and chemical properties, most likely involving tedious sample preparation to sandwich the particles in epoxy, followed by Focused Ion Beam (FIB) milling and lift out. Mixtures of TNT with 20% Al/GO showed enhanced microsecond- and millisecond-timescale energy release compared to TNT+Al mixtures. Increased microsecond-timescale energy release is expected to result in increased detonation performance, i.e., higher detonation velocities (shattering ability) and/or Gurney velocities (metal-pushing ability), while increased millisecond-timescale energy release is expected to result in increased blast effects (late-time impulse). Optimization of the formulation to achieve a better oxygen balance and improve performance is necessary. The predicted performance enhancements must then be confirmed with large-scale detonation testing.

## 5.0 REFERENCES

[1] Davari, S.A., Gottfried, J.L., Liu, C., Ribeiro, E.L., Duscher, G., Mukherjee, D. Graphitic-coated Al nanoparticles manufactured as superior energetic materials via laser ablation synthesis in organic solvents. Appl. Surf. Sci., 473:156-163, 2019.

[2] Gottfried, J.L., Smith, D.K., Wu, C.-C., Pantoya, M.L. Improving the explosive performance of aluminum nanoparticles with Aluminum Iodate Hexahydrate (AIH). Scientific Reports, 8: 8036, 2018.

[3] Miller, K.K., Gottfried, J.L., Walck, S.D., Pantoya, M.L., Wu, C.-C. Plasma surface treatment of aluminum nanoparticles for energetic material applications. Combust. Flame, 206:211-213, 2019.

[4] Wainwright, E.R., Dean, S.W., Lakshman, S.V., Weihs, T.P., Gottfried, J.L. Evaluating compositional effects on the laser-induced combustion and shock velocities of Al/Zr-based composite fuels. Combust. Flame, 213:357-368, 2019.

[5] Anderson, P.E., Cook, P., Davis, A., Mychajlonka, K. The effect of binder systems on early aluminum reaction in detonations. Propellants Explos. Pyrotech., 38:486-494, 2013.

[6] Yarrington, C.D., Son, S.F., Foley, T.J., Obrey, S.J., Pacheco, A.N. Nano aluminum energetics: The effect of synthesis method on morphology and combustion performance. Propellants Explos. Pyrotech., 36:551-557, 2011.

[7] Zha, M., Lv, X., Ma, Z., Zhang, L., Zhao, F., Xu, S., Xu, H. Effect of particle size on reactivity and combustion characteristics of aluminum nanoparticles. Combust. Sci. Technol., 187:1036-1043, 2015.

[8] Gottfried, J.L. Laser-induced plasma chemistry of the explosive RDX with various metallic nanoparticles. Appl. Opt., 51:B13-B21, 2012.

[9] Gottfried, J.L., Bukowski, E.J. Laser-shocked energetic materials with metal additives: evaluation of chemistry and detonation performance. Appl. Opt., 56:B47-B57, 2017.

[10] Krishnan, D., Kim, F., Luo, J., Cruz-Silva, R., Cote, L.J., Jang, H.D., Huang, J. Energetic graphene oxide: Challenges and opportunities. Nano Today, 7:137-152, 2012.

[11] Zhu, Y., Murali, S., Cai, W., Li, X., Suk, J.W., Potts, J.R., Ruoff, R.S. Graphene and graphene oxide: Synthesis, properties, and applications. Adv. Mater., 22:3906-3924, 2010.

[12] Singh, R.K., Kumar, R., Singh, D.P. Graphene oxide: Strategies for synthesis, reduction and frontier applications, RSC Advances, 6:64993-65011, 2016.

[13] Jiang, Y., Deng, S., Hong, S., Zhao, J., Huang, S., Wu, C.-C., Gottfried, J.L., Nomura, K.-i., Li, Y., Tiwari, S.C., Kalia, R.K., Vashishta, P., Nakano, A., Zheng, X. Energetic performance of optically activated aluminum/graphene oxide composites. ACS Nano, 12:11366-11375, 2018.

[14] Dreyer, D.R., Park, S., Bielawski, C.W., Ruoff, R.S. The chemistry of graphene oxide. Chemical Society Reviews, 39:228-240, 2010.

[15] Gao, W. The Chemistry of Graphene Oxide, in: W. Gao (Ed.) Graphene Oxide: Reduction Recipes, Spectroscopy, and Applications. Springer International Publishing, Cham, 2015, pp. 61-95, 2015.

[16] Pyun, J. Graphene oxide as catalyst: application of carbon materials beyond nanotechnology. Angew. Chem. Int. Ed., 50:46-48, 2011.

[17] Dreyer, D.R., Todd, A.D., Bielawski, C.W. Harnessing the chemistry of graphene oxide. Chem. Soc. Rev., 43:5288-5301, 2014.

[18] Adeel, M., Bilal, M., Rasheed, T., Sharma, A., Iqbal, H.M.N. Graphene and graphene oxide: Functionalization and nano-bio-catalytic system for enzyme immobilization and biotechnological perspective. Int. J. Bio. Macromol., 120:1430-1440, 2018.

[19] Singh, S.B., Hussain, C.M. Nano-graphene as groundbreaking miracle material: Catalytic and commercial perspectives. ChemistrySelect, 3:9533-9544, 2018.

[20] Ahmad, H., Fan, M., Hui, D. Graphene oxide incorporated functional materials: A review. Composites Part B, 145:270-280, 2018.

[21] Campisciano, V., Gruttadauria, M., Giacalone, F. Modified nanocarbons for catalysis. ChemCatChem, 11:90-133, 2019.

[22] Xiangjun, P., Xianyun, X., Fujiang, H., Qian, L., Liangxian, L. Graphene oxide and its derivatives: Their synthesis and use in organic synthesis. Current Org. Chem., 23:188-204, 2019.

[23] Brodie, XIII, B.C. On the atomic weight of graphite. Philos. Trans. R. Soc. Lond., 149:249-259, 1859.

[24] Croft, R.C. Lamellar compounds of graphite. Quarterly Reviews, Chem. Soc., 14:1-45, 1960.

[25] Boehm, H.P., Scholz, W. Der "Verpuffungspunkt" des graphitoxids. Zeitschrift für anorganische und allgemeine Chemie, 335:74-79, 1965.

[26] Jimenez, P.S.V. Thermal decomposition of graphite oxidation products DSC studies of internal combustion of graphite oxide. Mater. Res. Bull., 22:601-608, 1987.

[27] Sabourin, J.L., Dabbs, D.M., Yetter, R.A., Dryer, F.L., Aksay, I.A. Functionalized graphene sheet colloids for enhanced fuel/propellant combustion. ACS Nano, 3:3945-3954, 2009.

[28] Kim, F., Luo, J., Cruz-Silva, R., Cote, L.J., Sohn, K., Huang, J. Self-propagating domino-like reactions in oxidized graphite. Adv. Funct. Mater., 20:2867-2873, 2010.

[29] Li, R., Wang, J., Shen, J.P., Hua, C., Yang, G.C. Preparation and characterization of insensitive HMX/graphene oxide composites. Propellants Explos., Pyrotech., 38:798-804, 2013.

[30] Zhang, X., Hikal, W.M., Zhang, Y., Bhattacharia, S.K., Li, L., Panditrao, S., Wang, S., Weeks, B.L. Direct laser initiation and improved thermal stability of nitrocellulose/graphene oxide nanocomposites. Appl. Phys. Lett., 102:141905, 2013.

[31] Zhang, C., Wen, Y., Xue, X. Self-Enhanced Catalytic Activities of functionalized graphene sheets in the combustion of nitromethane: Molecular Dynamic simulations by molecular reactive force field. ACS Appl. Mater. & Interfaces, 6:12235-12244, 2014.

[32] Liu, J., Ren, H., Jiao, Q.-J., Yu, L. The influence of GO/RGO on the thermal decomposition of HNIW. Integrated Ferroelectrics, 152:127-136, 2014.

[33] Yu, L., Ren, H., Guo, X.-y., Jiang, X.-b., Jiao, Q.-j. A novel e-HNIW-based insensitive high explosive incorporated with reduced graphene oxide. J. Thermal Anal. Calorim., 117:1187-1199, 2014.

[34] Qiu, Y., Guo, F., Hurt, R., Külaots, I. Explosive thermal reduction of graphene oxide-based materials: Mechanism and safety implications. Carbon, 72:215-223, 2014.

[35] Thiruvengadathan, R., Chung, S.W., Basuray, S., Balasubramanian, B., Staley, C.S., Gangopadhyay, K., Gangopadhyay, S. A versatile self-assembly approach toward high performance nanoenergetic composite using functionalized graphene. Langmuir, 30:6556-6564, 2014.

[36] Thiruvengadathan, R., Staley, C., Geeson, J.M., Chung, S., Raymond, K.E., Gangopadhyay, K., Gangopadhyay, S. Enhanced combustion characteristics of bismuth trioxide-aluminum nanocomposites prepared through graphene oxide directed self-assembly. Propellants Explos. Pyrotech., 40:729-734, 2015.

[37] Chen, Y.N., Egan, G.C., Wan, J.Y., Zhu, S.Z., Jacob, R.J., Zhou, W.B., Dai, J.Q., Wang, Y.B., Danner, V.A., Yao, Y.G., Fu, K., Wang, Y.B., Bao, W.Z., Li, T., Zachariah, M.R., Hu, L.B. Ultra-fast self-assembly and stabilization of reactive nanoparticles in reduced graphene oxide films. Nat. Commun., 7:12332, 2016.

[38] Qiu, Y., Collin, F., Hurt, R.H., Külaots, I. Thermochemistry and kinetics of graphite oxide exothermic decomposition for safety in large-scale storage and processing. Carbon, 96:20-28, 2016.

[39] Memon, N.K., McBain, A.W., Son, S.F. Graphene oxide/ammonium perchlorate composite material for use in solid propellants. J. Propul. Power, 32:682-686, 2016.

[40] Wang, J., Ye, B., An, C., Wu, B., Li, H., Wei, Y. Preparation and properties of surface-coated hmx with viton and graphene oxide. J. Energ. Mat., 34:235-245, 2016.

[41] Yan, Q.-L., Gozin, M., Zhao, F.-Q., Cohen, A., Pang, S.-P. Highly energetic compositions based on functionalized carbon nanomaterials. Nanoscale, 8:4799-4851, 2016.

[42] Yan, N., Qin, L., Hao, H., Hui, L., Zhao, F., Feng, H. Iron oxide/aluminum/graphene energetic nanocomposites synthesized by atomic layer deposition: Enhanced energy release and reduced electrostatic ignition hazard, Appl. Surf. Sci., 408:51-59, 2017.

[43] Yan, N., Qin, L., Li, J., Zhao, F., Feng, H. Atomic layer deposition of iron oxide on reduced graphene oxide and its catalytic activity in the thermal decomposition of ammonium perchlorate. Appl. Surf. Sci., 451:155-161, 2018.

[44] Tao, Y., Zhang, J., Yang, Y., Wu, H., Hu, L., Dong, X., Lu, J., Guo, S. Metastable intermolecular composites of Al and CuO nanoparticles assembled with graphene quantum dots. RSC Advances, 7:1718-1723, 2017.

[45] Wang, J., Chen, S., Yao, Q., Jin, S., Zhao, S., Yu, Z., Li, J., Shu, Q. Preparation, characterization, thermal evaluation and sensitivities of TKX-50/GO composite. Propellants Explos. Pyrotech., 42:1-8, 2017.

[46] An, T., He, W., Chen, S.-W., Zuo, B.-L., Qi, X.-F., Zhao, F.-Q., Luo, Y., Yan, Q.-L. Thermal behavior and thermolysis mechanisms of ammonium perchlorate under the effects of graphene oxide-doped complexes of triaminoguanidine. J. Phys. Chem. C, 122:26956-26964, 2018.

[47] Lyu, J.-Y., Chen, S., He, W., Zhang, X.-X., Tang, D.-y., Liu, P.-J., Yan, Q.-L. Fabrication of high-performance graphene oxide doped PVDF/CuO/Al nanocomposites via electrospinning. Chem. Eng. J., 368:129-137, 2019.

[48] Chen, S., He, W., Luo, C.-J., An, T., Chen, J., Yang, Y., Liu, P.-J., Yan, Q.-L. Thermal behavior of graphene oxide and its stabilization effects on transition metal complexes of triaminoguanidine. J. Hazard. Mater., 368:404-411, 2019.

[49] Lakhe, P., Kulhanek, D.L., Sun, W., Zhang, B., Green, M.J., Mannan, M.S. Calorimetry of explosive thermal decomposition of graphite oxide. J. Hazard. Mater., 366:275-281, 2019.

[50] Zhang, C., Fu, X., Yan, Q., Li, J., Fan, X., Zhang, G. Study on the thermal decomposition mechanism of graphene oxide functionalized with triaminoguanidine (GO-TAG) by molecular reactive dynamics and experiments. RSC Advances, 9:33268-33281, 2019.

[51] Chen, S., An, T., Gao, Y., Lyu, J.-Y., Tang, D.-Y., Zhang, X.-X., Zhao, F., Yan, Q.-L. Gaseous products evolution analyses for catalytic decomposition of AP by graphene-based additives, Nanomaterials, 9:801, 2019.

[52] Cheng, J., Yan, J., Wang, L., Zhang, R., Liu, Z., Wang, R., Li, Z. Functionalization graphene oxide with energetic groups as a new family of metal-free and energetic burning rate catalysts and desensitizers for ammonium perchlorate. J. Thermal Anal. Calorim., 140:2111-2122, 2020.

[53] Hanafi, S., Trache, D., He, W., Xie, W.-X., Mezroua, A., Yan, Q.-L. Thermostable energetic coordination polymers based on functionalized go and their catalytic effects on the decomposition of AP and RDX. J. Phys. Chem. C, 124:5182-5195, 2020.

[54] Huang, B., Xue, Z., Chen, S., Chen, J., Li, X., Xu, K., Yan, Q.-L. Stabilization of e-CL-20 crystals by a minor interfacial doping of polydopamine-coated graphene oxide. Appl. Surf. Sci., 510:145454, 2020.

[55] Qi, X., Chen, S., Liu, X., Yan, N., Jin, B., Liu, P., Yan, Q.-L. Comparative study on compatibility of graphene-based catalysts with energetic ingredients by using DSC and VST methods. J. Thermal Anal. Calorim., in press (2020) https://doi.org/10.1007/s10973-020-09646-3, 2020.

[56] Jiang, Y., Deng, S., Hong, S., Tiwari, S., Chen, H., Nomura, K.-i., Kalia, R.K., Nakano, A., Vashishta, P., Zachariah, M.R., Zheng, X. Synergistically chemical and thermal coupling between graphene oxide and graphene fluoride for enhancing aluminum combustion. ACS Appl. Mater. & Interfaces, 12:7451-7458, 2020.

[57] Gottfried, J.L. Influence of exothermic chemical reactions on laser-induced shock waves. Phys. Chem. Chem. Phys., 16:21452-21466, 2014.

[58] Gottfried, J.L. Laboratory-scale method for estimating explosive performance from laser-induced shock waves. Propellants Explos. Pyrotech., 40:674–681, 2015.

[59] Collins, E.S., Gottfried, J.L. Laser-induced deflagration for the characterization of energetic materials. Propellants Explos. Pyrotech., 42:592-602, 2017.

[60] Gottfried, J.L., Klapötke, T.M., Witkowski, T.G. Estimated detonation velocities for TKX-50, MAD-X1, BDNAPM, BTNPM, TKX-55 and DAAF using the laser-induced air shock from energetic materials technique. Propellants Explos. Pyrotech., 42:353-359, 2017.

[61] Gottfried, J.L., Dean, S.W., Collins, E.S., Wu, C.-C. Estimating the relative energy content of reactive materials using nanosecond-pulsed laser ablation. MRS Adv., 3:875-886, 2018.

[62] Settles, G.S. Schlieren and Shadowgraph Techniques. Springer-Verlag, New York, 2001.

[63] Cremers, D.A., Radziemski, L.J. Handbook of Laser-Induced Breakdown Spectroscopy, 2nd ed. John Wiley & Sons, Ltd., Singapore, 2013.

[64] Serrano, J., Cabalín, L.M., Moros, J., Laserna, J.J. Potential of laser-induced breakdown spectroscopy for discrimination of nano-sized carbon materials. Insights on the optical characterization of graphene, Spectrochim. Acta, Part B, 97:105-112, 2014.

[65] De Lucia Jr., F.C., Gottfried, J.L. Characterization of a series of nitrogen-rich molecules using laser-induced breakdown spectroscopy. Propellants Explos. Pyrotech., 35:268-277, 2010.

[66] Shen, B., Lu, D., Zhai, W., Zheng, W. Synthesis of graphene by low-temperature exfoliation and reduction of graphite oxide under ambient atmosphere. J. Mater. Chem. C, 1:50-53, 2013.

[67] Medhekar, N.V., Ramasubramaniam, A., Ruoff, R.S., Shenoy, V.B. Hydrogen bond networks in graphene oxide composite paper: Structure and mechanical properties. ACS Nano, 4:2300-2306, 2010.

[68] Jin, M., Jeong, H.-K., Kim, T.-H., So, K.P., Cui, Y., Yu, W.J., Ra, E.J., Lee, Y.H. Synthesis and systematic characterization of functionalized graphene sheets generated by thermal exfoliation at low temperature. J. Phys. D, 43:275402, 2010.